Plasmon-induced magnetization of metallic nanostructures

Igor I. Smolyaninov,[1] Christopher C. Davis,[1] Vera N. Smolyaninova,[2] David Schaefer,[2] Jill Elliott,[3] and Anatoly V. Zayats[3]
[1]*Department of Electrical and Computer Engineering, University of Maryland, College Park, Maryland 20742, USA*
[2]*Department of Physics, Astronomy and Geosciences, Towson University, Towson, Maryland 21252, USA*
[3]*School of Mathematics and Physics, The Queen's University of Belfast, Belfast, BT7 1NN United Kingdom*
(Received 24 August 2004; revised manuscript received 13 October 2004; published 28 January 2005)

Plasmon-induced magnetism of nanostructured metallic samples has been studied. Magnetic force microscopy measurements show that magnetization of a nanohole array can be achieved by illumination of the structure at the wavelengths corresponding to various surface plasmon excitations. This second-order nonlinear optical effect appears to affect propagation of light through an array of such nanoholes in a gold film as observed by spectroscopic measurements in external magnetic field. This effect can find numerous applications in magneto-optical data storage and optical communication and computing.

DOI: 10.1103/PhysRevB.71.035425 PACS number(s): 78.67.−n, 78.66.Bz

I. INTRODUCTION

In transparent dielectric materials a quantum of electromagnetic excitation (light) is a photon. However, in the case of metals photons are not a good approximation, and coupled states of photons and the collective excitations of conductivity electrons—surface plasmons (SP) close to a metal surface should be considered to understand optical properties, which are called surface plasmon polaritons (SPP). Since photons do not penetrate deep into a metal ($\mathrm{Re}\,\varepsilon_m < 0$), in many cases optical properties of metallic materials and structures are determined by surface plasmon polaritons (propagating surface waves) and other surface plasmon excitations (localized and/or cylindrical surface plasmons) depending on the metal geometry.[1] Unusual optical properties of metallic nanowires and nanoholes stemming from the surface plasmon properties are the topic of considerable current interest, due to the strong drive toward development of a new generation of nano-optical devices for high-density optical data storage, classical and quantum optical communications, and computing.

Anomalously high optical transmission of an array of nanoholes in a metal film is one of the effects which are strongly affected by surface plasmon modes.[2,3] Such an enhanced transmission is related to the properties of the SPP Bloch modes on a periodically structured surface, which are excited due to diffraction on a periodic structure, as well as cylindrical and localized surface plasmons in holes, depending on the structure parameters. When incident photons are coupled to surface plasmon excitations in the nanostructure, light in a form of surface plasmons gets through a film and then is decoupled back to photons on the opposite side of the film. Control over surface plasmons provides means to control optical properties of the metallic nanostructures.[4] In turn, properties of the electromagnetic excitations in such nanostructures depend on the nanostructure geometry and size.

The nano-optics effect considered above is just one example among a large number of unusual physical phenomena in which optics meets mesoscopic physics. Magnetic and transport properties of mesoscopic systems are the topics of very active current research,[5] due to the strong drive toward development of nanodevices and quantum computing. However, there still exist some contradictions between mesoscopic theories and experiment (see Ref. 6 for example). One of the missing intrinsic elements in many current experimental and theoretical studies is the effect of surface plasmons on the transport and magnetic properties of mesoscopic metallic samples, such as wires, rings, and various other shapes. The importance of surface plasmons in mesoscopic phenomena is clear from the recent paper[7] and from the following qualitative consideration.

The usual justification for not considering surface plasmons in low-temperature measurements is that the efficiency of excitation of surface plasmons is small if the sample size is of the order of a few micrometers. However, even if there are no real SP quanta in the system, the zero-point fluctuations of the electromagnetic field of all the possible plasmon modes in the system have to be considered. The importance of zero-point fluctuations in mesoscopic systems clearly manifests itself in the observations of negative vacuum energy density between metal plates separated by submicrometer distances (the Casimir effect; see Ref. 8, for example). The energy density in such a mesoscopic cavity depends on the dielectric constant of the material between the metal plates. A mesoscopic metallic sample constitutes a similar mesoscopic resonator for surface plasmons. As has been shown in numerous papers, the magnetic field produces substantial modifications of the surface plasmon dispersion law via modification of the dielectric tensor of the metal,[9] and via the Aharonov–Bohm (AB) effect (the frequencies of surface plasmon modes in nanotubes and mesoscopic rings change periodically by about 10% due to the AB effect[10]). Thus, the magnetic field applied to a mesoscopic sample effectively changes its "dielectric constant" as seen by the surface plasmons, and hence, changes the zero-point energy of the plasmon field. This fact may be interpreted as an additional vacuum contribution to the magnetic moment $\mu_{vac} = -\partial E_0/\partial H$ of the metal sample, where E_0 is the zero-point energy of surface plasmon vacuum. According to the results presented in Refs. 9 and 10, this vacuum contribution may be quite large because of the rather large magnetic moments $-\hbar\partial\omega/\partial H \sim \mu_B$ of the individual plasmon modes, and be-

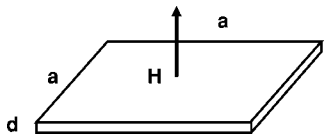

FIG. 1. Model geometry for the calculations of the magnetic response of surface plasmon vacuum in the case of a square $a \times a$ region of a thin metal film with thickness $d \ll a$ in an applied perpendicular magnetic field H.

cause of the very large total number of plasmon modes supported by a mesoscopic sample.

In this paper we study the plasmon-induced magnetism of nanostructured metallic samples. We calculate the plasmon zero-point energy of some metallic mesoscopic samples with simple geometries in an external magnetic field. The magnetic response of the plasmon vacuum of these samples appears to be rather large and diamagnetic. In thin films this predicted surface vacuum diamagnetism appears to be at least of the same order of magnitude as the magnetism of the bulk electrons. Thus, a type of magnetism shown by thin metallic samples, which is complementary to the well-known Pauli paramagnetic and Landau diamagnetic contributions to the magnetism of electron gas, is demonstrated. The plasmon-induced magnetism of such samples may be enhanced by external illumination with resonant light. We report on the experiments in which illumination of nanohole arrays in metal films induced their magnetization, which has been observed directly with a magnetic force microscope (MFM). This effect allows one to control optical transmission through such structures with an applied external magnetic field or to illuminate the sample at certain wavelengths to induce magnetization in an initially nonmagnetic nanostructure. Such an unusual "magnetic" effect has been observed in the experiments on the magnetic-field-induced changes in the transmission of an array of cylindrical nanoholes. It seems that the nonlinear optical coupling between the cylindrical plasmons of different nanoholes in the array may be described as magnetic interactions in a two-dimensional lattice of magnetic moments, which is reminiscent of the Ising model. This effect may have profound implications in high-density magneto-optical data storage as well as classical and quantum optical communications and computing. It might provide a route to the development of optical metamaterials with negative magnetic permeability at optical frequencies if coherent excitation of cylindrical surface plasmons can be achieved.

II. PLASMON-INDUCED MAGNETIZM OF MESOSCOPIC SAMPLES

Although quanta of electromagnetic field (photons) carry angular momentum, they do not possess magnetic moment in vacuum. This fact may not be true in every medium. Let us consider the magnetic response of the surface plasmon vacuum of a square $a \times a$ region of a thin metal film with thickness $d \ll a$ to an applied magnetic field H (Fig. 1). Let us start by considering the SPP dispersion law, which propagates along the metal-dielectric interface in zero magnetic

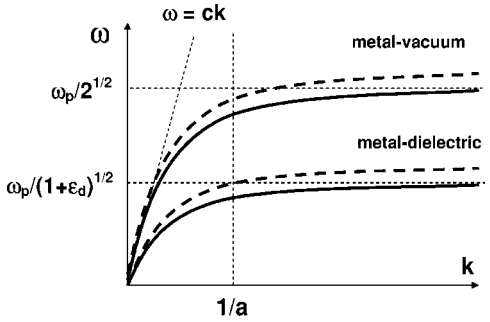

FIG. 2. SPP dispersion law for the cases of metal-vacuum and metal-dielectric interfaces in zero magnetic field (solid lines) and in the magnetic field applied perpendicular to the film surface (dashed lines). At large SPP wave vectors k the changes in surface plasmon frequency in the applied magnetic field do not depend on k.

field. The SP field decays exponentially both inside the metal and the dielectric. Let us assume that both metal and dielectric completely fill the respective $z<0$ and $z>0$ half-spaces. In such a case the dispersion law can be written as[1]

$$k^2 = \frac{\omega^2}{c^2}\frac{\epsilon_d \epsilon_m(\omega)}{\epsilon_d + \epsilon_m(\omega)}, \tag{1}$$

where we will assume that $\epsilon_m = 1 - \omega_p^2/\omega^2$ according to the Drude model, and ω_p is the plasma frequency of the metal. This dispersion law is shown in Fig. 2 for the cases of metal-vacuum and metal-dielectric interfaces. It starts near the "light line" in the respective dielectric at low frequencies and approaches asymptotically $\omega = \omega_p/(1+\epsilon_d)^{1/2}$ at very large wave vectors. The latter frequency corresponds to the so-called surface plasmon resonance. Under the surface plasmon resonance conditions both phase and group velocity is zero, and the surface charge and the normal component of the electric field diverge. While the dispersion relation (1) is modified in the general case of a lossy metal film, the approximation used in (1) remains good in the case of a symmetric experimental geometry in which the dielectric constants of the dielectric on both sides of the metal film coincide. Since at every wave vector the SPP dispersion law is located to the right of the light line, the SPPs of the plane metal-dielectric interface are decoupled from the free-space photons due to the momentum conservation law.

We are mostly interested in the region of the SPP dispersion law near the SP resonance. The corrections to surface plasmon frequency in an applied magnetic field in the so-called nonretarded electrostatic approximation (which is of the most interest to us) were calculated by Chiu and Quinn.[9] In this approximation SPPs have zero dispersion $d\omega/dk = 0$, which makes summation over all the plasmon modes extremely easy. These modes correspond to the SPPs with large wave vectors, which propagate in the xy plane along the planar metal-dielectric interface. Assuming that SPP propagates in the y direction, the eigenfrequencies of surface plasmons in magnetic field are given by[9]

$$\omega = \begin{cases} (\omega_p^2 + \omega_c^2)^{1/2}/2^{1/2} & \text{for } H \perp x \\ (\omega_p^2 + \omega_c^2)^{1/2}/2^{1/2} \pm \omega_c/2 & \text{for } H \parallel x, \end{cases} \tag{2}$$

where $\omega_c = eH/mc$ is the cyclotron frequency, and the sign of $\omega_c/2$ term is determined by the propagation direction. The

magnetic moment μ of the SPP quanta can be determined from the basic thermodynamic definition of a magnetic moment of a system as follows:

$$\mu = -\hbar\left(\frac{\partial\omega}{\partial H}\right)_{H=0}. \tag{3}$$

Thus, SPP quanta have magnetic moments of the order of the Bohr magneton $\mu_B = e\hbar/2mc$, which are normal to their propagation direction ($H \| x$). We should point out that the just introduced magnetic moment of a plasmon represents a second order nonlinear optical effect. This is evident from Eq. (2), which basically describes mixing of the ac field of the plasmon with the dc magnetic field. Such second-order mixing produces terms of the order of $\chi^{(2)}E_p^2 H$ in the plasmon field energy density, where the E_p^2 factor represents the terms quadratic in the electric field of the surface plasmon and $\chi^{(2)}$ can be considered as the generalized second-order susceptibility that includes also magneto-optical effects (similar to the light-induced magnetization of transparent optically active media[11]). As a result, the plasmon energy acquires contribution, which is linear in H. This contribution is proportional to $\chi^{(2)}E_p^2$. These terms describe both second harmonic and photon drag dc electric fields as well as linear magneto-optical effects due to surface plasmons near the metal interface. We should note that the inversion symmetry is broken near every interface, so that such $\chi^{(2)}E_p^2$ terms are always present at the surface. The fact that this effect is rather noticeable is also a direct consequence of the zero dispersion $d\omega/dk = 0$ of surface plasmons with large momenta k: according to Eq. (2), application of external magnetic field changes frequency (and, hence, energy) of such plasmons. We should also point out that there is no contradiction between this statement and the fact that external magnetic field cannot change the total energy of a classical system of electric charges. Even though plasmons are classical electron density waves, they cannot be isolated from the rest of the metal, and magnetism in metals is an essentially quantum mechanical phenomenon. Similarly, photons in regular magneto-optical materials mostly respond to the external magnetic field by changing their momenta (because of the magnetic-field-induced change of the refractive index). They can also exhibit second-order mixing with an external magnetic field and, hence, dc magnetism.[11] However, unlike plasmons, photons in transparent materials are highly delocalized, and such a dc magnetic field should be small. The magnetism of surface plasmons is much more pronounced because they are highly confined near the interface, and in addition plasmons may exhibit localization around topographical surface features.[1]

Let us initially consider the most simple case of magnetic field H applied perpendicular to the metal film bounded by vacuum. At large SPP wave vectors k the surface plasmon frequency

$$\omega_{sp} \approx [(\omega_p^2 + \omega_c^2)/2]^{1/2} \tag{4}$$

does not depend on k (Fig. 2), where ω_p and $\omega_c = eH/mc$ are the plasma and cyclotron frequencies, respectively.[9] As a result, all the surface plasmon modes have the magnetic moment $-\hbar\partial\omega/\partial H$ induced by the externally applied dc magnetic field, and the total magnetic moment of the SP vacuum can be written as

$$\mu_{vac} \approx -\mu_B/2^{1/2}\sum_k \omega_c/\omega_p, \tag{5}$$

where μ_B is the Bohr magneton, and summation has to be done over all the plasmon modes of the square region of the thin metal film under consideration. The surface plasmon eigenmodes of this square region are defined by the two-component wave vector $(k_x, k_y) = \pi/a \times (n_x, n_y)$, where n_x and n_y are integer. Due to Landau damping[12] the summation over all possible surface plasmon wave vectors has to be cutoff at $|k_{max}| \sim k_F$ (the electron Fermi momentum). Thus, the total number of SP modes on the top and bottom interfaces of the metal film is roughly $8(k_F a/\pi)^2$, and

$$\mu_{vac} \approx -8a^2 n_e^{2/3}(\omega_c/\omega_p)\mu_B. \tag{6}$$

For thin metal films this surface vacuum diamagnetism is at least of the same order of magnitude as the contribution of the bulk electrons. Detailed description of various contributions to the magnetism of metallic samples can be found, for example, in Ref. 13. The dominating mechanism of the magnetism of conductivity electrons is the paramagnetic contribution obtained by Pauli[14] as

$$\chi_e^{pm} = \frac{3^{1/3} m\mu_B^2}{\pi^{4/3}\hbar^2} n_e^{1/3}, \tag{7}$$

where m is the electron mass. The diamagnetic contribution obtained by Landau[15] is usually smaller by approximately three times.[13] Thus, we only need to compare the magnitudes of the Pauli paramagnetic contribution and the surface plasmon vacuum contribution to the electron magnetism of our thin metal film sample. Let us assume the free-electron model value for the plasma frequency of electron gas in the metal[1]

$$\omega_p^2 = \frac{4\pi e^2 n_e}{m} \tag{8}$$

and compare these two contributions. The Pauli paramagnetic moment of our sample can be written as follows:

$$\mu_{pm} \approx a^2 n_e^{2/3}\omega_c \frac{3^{1/3} md}{2\pi^{4/3}\hbar n_e^{1/3}}\mu_B = 8a^2 n_e^{2/3}(\omega_c/\omega_d)\mu_B, \tag{9}$$

where d is the film thickness, and some characteristic frequency $\omega_d = 16\pi^{4/3}\hbar n_e^{1/3}/(3^{1/3}md)$ is introduced. From this expression we immediately see that at small film thicknesses d, such that $\omega_p \sim \omega_d$, Pauli paramagnetic and surface plasmon vacuum diamagnetic contributions have the same order of magnitude. The characteristic film thickness necessary for this situation to occur can be written as

$$d \sim \frac{16\pi^{4/3}\hbar n_e^{1/3}}{3^{1/3} m\omega_p} \sim \frac{8\pi^{5/6}\hbar}{3^{1/3} m^{1/2} e n_e^{1/6}} \sim 2 \text{ nm}. \tag{10}$$

Thus, according to this simple estimate Pauli paramagnetic and surface plasmon vacuum diamagnetic contributions to the magnetism of a thin film sample would be approxi-

mately equal at $d \sim 2$ nm. Moreover, the contributions of Landau diamagnetism and plasmon vacuum diamagnetism should be about the same at $d \sim 6$ nm. As a result, experimental measurements of the magnetic response of mesoscopic thin film samples performed as a function of film thickness in the 2–20-nm range have reasonable chance of detecting the surface plasmon vacuum diamagnetism. We should also point out that in reality the vacuum diamagnetic moment may be at least an order of magnitude larger than the value determined by Eq. (6), since the cutoff wave vector is known only by an order of magnitude. In addition, magnetic response measurements may be performed as a function of the dielectric constant of the substrate and/or absorbed layer on the interfaces of the metal film. According to Chiu and Quinn,[9] in the presence of a dielectric layer on the metal surface and at large SPP wave vectors k the surface plasmon frequency in a magnetic field perpendicular to the SPP propagation direction is given by

$$\omega_{sp} \approx [(\epsilon_d^{-1}\omega_p^2 + \omega_c^2)/2]^{1/2}, \tag{11}$$

where ϵ_d is the dielectric constant of the layer. As a result, the magnetic moment of individual SP modes $-\hbar\partial\omega/\partial H$, and the total magnetic moment of the SP vacuum [defined by Eqs. (5) and (6)] are multiplied by the refractive index of the dielectric $n_d = \epsilon_d^{1/2}$. Since atomic monolayer quantities of the adsorbents are sufficient to shift the plasmon resonance,[1] such measurements may be very useful in separating the relative contribution of the vacuum diamagnetism into the overall magnetic response of the sample (since there is no reason why a thin absorbed layer would alter either Pauli or Landau contributions). In addition, increase of the overall effect by another factor of 2 or 3 means that even thicker metal films (few tens of nanometers) may be used to make a mesoscopic sample of interest. This additional increase in the scale of the film thickness also means that calculations of SP eigenfrequencies based on the macroscopic Maxwell equations are much more reliable.

Except for the extreme sensitivity to the absorbed layers, the vacuum diamagnetism described above looks similar to the Pauli and Landau contributions with respect to temperature changes. Since surface plasmon eigenfrequencies involved are of the order of a few electron volts, no considerable changes in the surface plasmon magnetic response may be expected from absolute zero up to the room temperature. The best candidates for vacuum diamagnetism observations may be the mesoscopic samples made of gold, silver, copper, or aluminum, since these metals exhibit very pronounced plasmon resonances.[1] Even in the presence of absorbed layers the vacuum diamagnetic contribution defined by Eq. (6) is rather small due to the small (ω_c/ω_p) factor. For a gold sample at $H=1$ T this ratio is $(\omega_c/\omega_p) \sim 10^{-4}$. Thus, a 1×1-μm^2 square sample would have a vacuum diamagnetic moment of $\sim 10^4 \mu_B$ at $H=1$ T, or a few tens of Bohr magnetons at $H=10$ G. However, similar sensitivity has been achieved recently by Deblock *et al.*[6] who reported measurements of the magnetic response of individual mesoscopic silver rings and obtained that the measured response of an individual silver ring is diamagnetic in the limit of zero magnetic field, which was not consistent with the available theoretical predictions. According to these measurements performed on an ensemble of 1.5×10^5 1×1-μm^{2}square silver rings with the thickness of 70 nm, the magnetic moment of an individual ring oscillates with the number of magnetic flux quanta with an amplitude of approximately $30\mu_B$ and the period of $\sim$20 G. Regardless of the nature of these oscillations, which we will briefly discuss later, the result of Deblock *et al.* for the unexpected diamagnetic response of an individual ring seams consistent with both the sign and the magnitude (according to Fig. 4 from Ref. 6, $\mu_{ring} \sim 10\mu_B$) of the vacuum diamagnetic contribution described earlier.

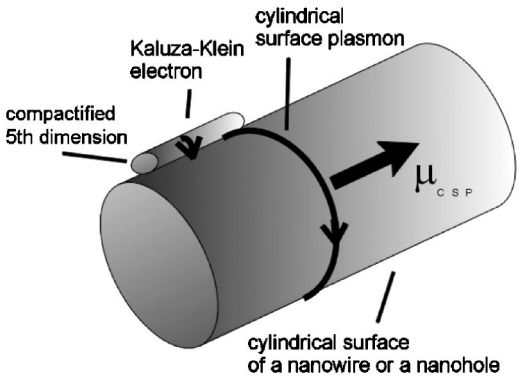

FIG. 3. Geometry of the cylindrical surface plasmon with angular momentum n on a surface of a metal nanowire or nanohole in a metal film. Symmetry between a cylindrical surface plasmon and an electron is illustrated: both excitations may be represented by a chiral mode of a massless field which is quantized over a compactified spatial coordinate.

Relatively weak effects of a plasmon vacuum magnetic response of nanostructured samples may be amplified considerably by external illumination. For example, resonant illumination of the nanohole array samples is known to be an efficient way of excitation of various surface plasmon modes.[2–4] While the magnetism of SPP Bloch modes on a periodically modulated surface of a metal film can be considered in the same way as the magnetism of SPP modes of the square sample in Fig. 1, the contribution of surface plasmons localized in and around the nanoholes need separate consideration.

Cylindrical surface plasmons (CSP) which exist on a cylindrical surface of a nanohole in metal film (or on the surface of a cylindrical wire) are described by the wave vector k_z related to CSP propagation in the axial direction of the cylinder, and the angular quantum number n related to the azimuthal CSP propagation (k_ϕ) along the cylinder circumference (Fig. 3). As a result, the CSP trajectory on a cylindrical surface can be represented as a spiral with the period determined by the CSP angular quantum number: for $n=0$ there is no angular momentum and such CSP is analogous to the surface plasmon on a plane surface propagating over the cylinder wall in the axial direction; for $n \gg 1$ CSPs strongly rotate around the cylinder and their spectrum converges to $\omega_p/2^{1/2}$ in the large wave vector limit. The magnetic moment μ of individual CSP quanta can be determined as

$$\mu = -\hbar\left(\frac{\partial\omega}{\partial H}\right)_{H=0} = -\frac{ea^2}{c}\left(\frac{\partial\omega}{\partial\phi}\right)_{\phi=0}, \tag{12}$$

where H is the external magnetic field applied in the axial direction, a is the cylinder radius, and ϕ is the number of magnetic flux quanta inside the cylinder. The estimation of CSP magnetic moment is easy to perform in the two limiting cases $n=0$ and $n\to\infty$ if the nonretarded electrostatic approximation is used. These states correspond to the SPP with large wave vectors, which propagate parallel and perpendicular to the axial magnetic field, respectively. In this case we can neglect the effects of curvature of the cylinder, and the results of Ref. 9 are reproduced: the eigenfrequencies of CSPs in magnetic field are given by

$$\omega = \begin{cases} (\omega_p^2+\omega_c^2)^{1/2}/2^{1/2} & \text{for } n=0 \\ (\omega_p^2+\omega_c^2)^{1/2}/2^{1/2} \pm \omega_c/2 & \text{for } n\neq 0. \end{cases} \tag{13}$$

It is evident that the $n=0$ plasmons do not have magnetic moments, while $n\neq 0$ CSP quanta have magnetic moments of the order of the Bohr's magneton μ_B. Exact values of the CSP magnetic moments can be determined by taking into account the effects of curvature of the cylinder, retardation, and the Aharonov–Bohm effect on the CSP dispersion. Analysis of the numerical calculations of the CSP dispersion for a number of different geometries reported in Refs. 10 and 16 indicates that the results of the simple qualitative estimate above remain valid in all these cases: CSPs with zero angular momentum have no magnetic moment, while $n\neq 0$ CSPs have $\mu\sim\mu_B$. Thus, individual quanta of the $n\neq 0$ CSP electromagnetic field behave like small magnets.

The $n\neq 0$ CSP modes in a nanowire or a nanohole are examples of plasmon modes which exhibit linear dependence of their frequencies on the applied magnetic field. Similar cases may be found in Refs. 9, 10, and 16. For example, if magnetic field is applied parallel to the metal film (in the x direction), then according to Chiu and Quinn[9] at large SPP wave vectors k, the surface plasmon frequency is given by

$$\omega_{sp} \approx \left[\left(\omega_p^2+\tfrac{1}{2}\omega_c^2\right)/2\right]^{1/2} \pm \tfrac{1}{2}\omega_c, \tag{14}$$

where the two signs correspond to plasmon propagation in the $\mp y$ direction. Such plasmon modes have magnetic moments $-\hbar\partial\omega/\partial H\sim\pm\mu_B$. In rotationally symmetric samples vacuum magnetic moments of these "left" and "right" modes compensate each other, so that only the contributions quadratic in the magnetic field are left in the expression for the total zero-point energy of the plasmon vacuum, and we would come up with an expression more or less similar to Eq. (6) for the vacuum magnetic moment. However, this may not be the case for an asymmetric sample. Considered in terms of nonlinear optics, the magnetic moment of a CSP mode which exhibits such a linear dependence of its frequency on the applied magnetic field should be treated as a second-order nonlinear optical effect similar to the light-induced magnetization of the transparent optically active media sometimes called the *inverse Faraday effect*.[11] The dc magnetic field generated by CSP excitation is proportional to the number of SP quanta excited in the sample, and hence, to the square of the fundamental field of the CSP. As such, this effect is the second-order nonlinear-optical effect, which is somewhat similar to the photon drag, and complementary to the generation of second harmonic which always takes place near metal interfaces. Even though the film material itself (gold) has a cubic lattice, and the grating of nanoholes is mirror symmetric, this effect is possible due to the broken inversion symmetry at the metal interface.

It is interesting to note that nonlinear optics of CSPs resembles the description of electrodynamics of electric charges in high energy physics theories which introduce compactified extra dimensions. In such theories the effective electric charge of each electromagnetic field mode is proportional to the component of this mode's momentum n in the compactified extra dimension, so that the electric charge conservation becomes a simple consequence of the momentum conservation law.[17] In a similar way, cylindrical surface plasmons of a nanowire or a nanohole may be considered as if they exist in a curved three-dimensional space-time defined by the metal interface, which in addition to an extended z coordinate, has a compactified angular ϕ dimension along the circumference of the cylinder (Fig. 3). As a result, similarity between the CSPs with $n\neq 0$ and Kaluza–Klein electrons becomes evident: both types of excitations are described by a respective quantized component of the angular momentum n along a compactified dimension. A detailed discussion of this analogy may be found in Ref. 7. If we recall that in addition to an electric charge, electrons posses a magnetic moment, this analogy becomes even more evident. Similar to electrons, cylindrical surface plasmons with nonzero angular momenta have nonzero magnetic moments as well.

Another potentially important (although separate) question is how the AB effect may affect the plasmon-induced magnetism of mesoscopic samples. Very recently Chaplik *et al.* demonstrated that the frequencies of surface plasmon modes in nanotubes and mesoscopic rings change periodically by about 10% due to the AB effect.[10] The reason for this effect is the fact that both Fermi energy and the polarization operator of the nanotubes and nanorings changes periodically with magnetic flux due to the periodic dependence of the single-particle spectrum on magnetic flux. These periodic changes lead to the periodic changes of the surface plasmon eigenfrequencies, which can be found by solving the Poisson equation. Thus, magnetic moments of these modes $-\hbar\partial\omega/\partial H$ experience periodic oscillations too. According to the results of numerical calculations by Chaplik *et al.*[10] the amplitude of these oscillations is of the order of μ_B for the zero-angular momentum ($n=0$) plasmon mode of a carbon nanotube at $ka=1$ [Fig. 2(b) from Ref. 10], while this mode does not have any angular momentum in zero magnetic field (for this mode $d\omega/dH=0$ at $H=0$ as is required by symmetry considerations earlier). Similar to the classical consideration for cylindrical surface plasmons with nonzero angular momentum, plasmons of the nanotube with $n\neq 0$ have nonzero AB-induced magnetic moments (Fig. 4 from Ref. 10). While exact numerical calculations for the total AB-induced vacuum magnetic moment would be rather cumbersome, because of the complicated dependencies of the frequencies of the plasmon modes with arbitrary n and k on the magnetic flux,[10] there is absolutely no reason for the total vacuum

magnetic moment not to experience periodic oscillations with the amplitude of a few μ_B due to the AB effect. Thus, the periodic small oscillations of the magnetic response of the silver rings observed by Deblock *et al.*[6] may also be at least partially attributed to the oscillations of plasmon vacuum magnetism.

III. EXPERIMENTAL OBSERVATIONS OF PLASMON-INDUCED MAGNETISM

The discussion in the previous section indicates that although rather weak, magnetism of surface plasmon polaritons and cylindrical surface plasmons should be detectable in the experiment. It may be detected either using mesoscopic transport measurements similar to a technique implemented in Ref. 6, or using optical transmission measurements in magnetic field. In addition, direct measurements of the plasmon-induced magnetic moments may be performed using high sensetivity MFM or a superconducting quantum interference device (SQUID) magnetometery.

Magnetic properties of CSPs should manifest themselves in the optical properties of cylindrical plasmons in the external magnetic field. Influence of the magnetic field on cylindrical surface plasmons possessing magnetic moments should lead to the change of the radiation spectrum associated with CSPs. Since cylindrical surface plasmons with large quantum numbers $n \gg 1$ have dispersion curves approaching, in the limit of large wave vectors, the surface plasmon frequency, it is these CSPs that will contribute most to the magnetic field effects near $\omega = \omega_p / 2^{1/2}$ due to their high density of states (since $d\omega/dk$ is small for $k \to \infty$). However, such CSPs cannot be excited directly by the incident light because of the difference in the wave vectors. A periodic array of cylindrical holes facilitates the excitation of CSPs in this spectral range due to diffraction effects.

The measurements of the effect of magnetic field on the spectrum of cylindrical surface plasmons (Fig. 4) strongly indicate the suggested magnetic behavior. The transmission spectra of a periodic array of cylindrical holes [the structure is shown in the inset in Fig. 4(a)] created in a 40-nm-thick gold film on a glass substrate using focused ion beam milling have been measured with [Fig. 4(b)] and without [Fig. 4(a)] applied 0.46-T magnetic field having component perpendicular to the film (parallel to the holes axis). The transmission spectrum of the array measured under the white light illumination without the applied magnetic field $T(0)$ has two major features in the spectral range of plasmonic excitations. The first one is the peak of the enhanced transmission around 500 nm wavelength, which corresponds to the Bloch surface plasmon polariton states on the gold-air interface. The detailed discussion of such Bloch states at the gold-air and gold-substrate interface can be found in Ref. 3. In general, the resonant SPP wave vectors $\vec{k}$ are given by integer multiples of the inverse vectors $(\vec{u}, \vec{q})$ of the two-dimensional periodic surface structure: $\vec{k} = m\vec{u} + n\vec{q}$, where m and n are integer. In case of the double-period structure in Fig. 4(a) the picture of Bloch states is somewhat more complicated because of the more complicated basis of the two-dimensional rectangular Brave lattice of the structure. However, the wide

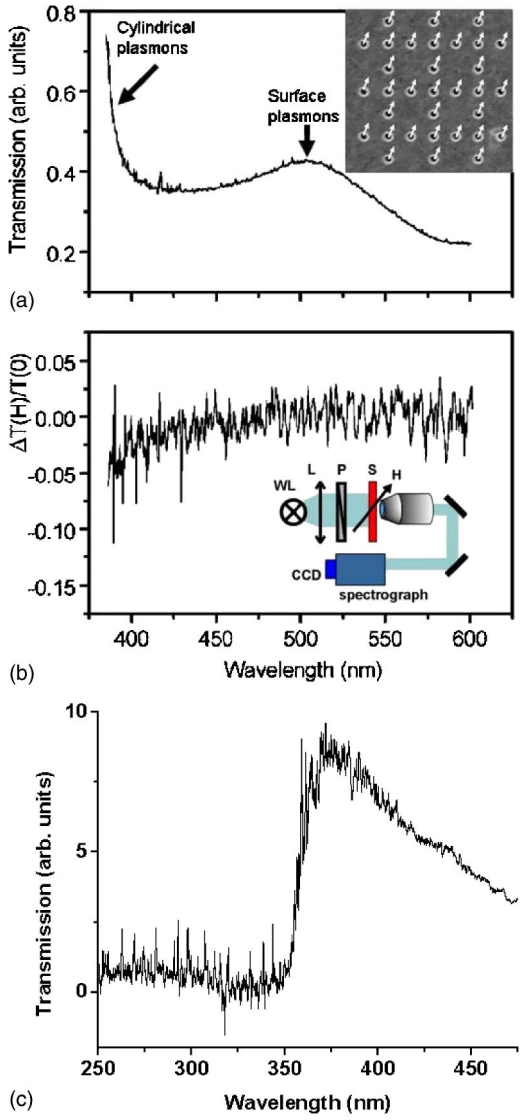

FIG. 4. (Color online) (a) Optical transmission $T(0)$ of the nanohole array without applied magnetic field. (b) Spectrum of the relative change $[T(H)-T(0)]T(0)$ of the optical transmission in the applied magnetic field. (c) Detailed measurements of the CSP spectrum around 400 nm obtained with a different UV-sensitized CCD spectrometer. The inset in (a) shows the electron microscope image of the double period nanostructure used for spectral measurements: the hole diameter is 150 nm, periodicity is $D_1 = 600$ nm and $D_2 = 1200$ nm. The presumed magnetic moments of CSPs are shown by the arrows. The inset in (b) shows experimental setup: WL-light source, L-lens, P-polariser, S-sample.

peak around 500 nm may be identified reasonably well with the combination of $(\pm 1, \pm 1)$, $(0, \pm 2)$, $(\pm 2, 0)$, etc. states of the $D_1 = 600$-nm lattice period of surface plasmon-polaritons on the gold-air interface of the nanohole array structure. The second spectral feature close to 400 nm [shown in more detail in Fig. 4(c), which was obtained by using a different charge coupled device (CCD) spectrometer that is much more sensitive in the UV spectral range] should at least partially correspond to the excitation and reradiation of cylindrical surface plasmons with large angular momenta in the holes. In this spectral range, the double period structure pro-

vides the excitation of surface plasmon polariton modes on a gold-air interface corresponding to higher in-plane diffraction orders which can then couple to the CSPs. The differential transmission $[T(H)-T(0)]/T(0)$ of the nanohole array in the applied magnetic field [Fig. 4(b)] in this spectral range was observed to depend on the applied magnetic field. Our data indicate a clear negative differential shift below 450 nm; in the longer-wavelength range no magnetic field induced effects was observed. Despite a significant noise level, which is unavoidable in differential measurements of small signals and which might lead to the difficulties in the identification of absolute zero of the differential signal, the overall signal-to-noise ratio in this spectral range is at least a factor of 3. We believe that this fact establishes statistically meaningful magnetooptical effect observation in the spectral range below 450 nm. On the other hand, the SPP-related transmission above 450 nm is not sensitive to magnetic field within our experimental precision. This weak magnetic field dependence corresponds well to the expected weak dependence of the CSP radiation on the applied magnetic field. According to Eq. (13), the CSP peak is supposed to experience some broadening due to the splitting of left and right CSP modes as well as possible coupling between CSPs in the hole array described below. This broadening of the CSP peak [located around 375 nm according to Fig. 4(c)] should lead to transmission changes around 400 nm, as detected in the experiment: the broadened peak extends more into the spectral range of measurements in Figs. 4(a) and 4(b).

It is also interesting to note that the nonlinear optical coupling between the CSPs in different nanoholes in the array may, in principle, be described as an effective magnetic exchange interaction in a two-dimensional lattice of magnetic moments. Similar to the exchange interaction of electrons in electronic magnetic materials, this effective interaction of plasmons results not from the direct interaction of their magnetic moments (which is rather weak), but from the statistics of plasmons. The CSPs are bosons, so they would "like" to be in the same orbital (and hence magnetic) state, due to their statistics, when excited by circular polarized coherent light: the probability of the new CSP to be excited in some particular orbital state is proportional to the number of CSP quanta already excited in this state. In order for this interaction to occur between the CSP states in neighboring nanoholes, the CSP states of these nanoholes should be coupled. Thus, the distance between the nanoholes in the array should be compatible with k_z^{-1} of the CSPs (k_z^{-1} defines the rate of the CSP field decay along the metal film surface; remember that z direction for CSPs was introduced as a direction perpendicular to the cylindrical surface). Once CSPs of individual nanoholes are coupled to each other, they become delocalized and form Bloch waves, which may propagate along the metal surface in a manner, which is similar to the propagation of regular SP Bloch waves over the perforated metal surface. As a result, the CSPs in such dense nanohole arrays experience rather strong effective exchange interaction, and a two-dimensional lattice of magnetic moments, which is reminiscent of the Ising model, is formed in the nanohole array as shown in the inset in Fig. 4(a). Thus, two-dimensional "photonic" magnetic materials may be introduced. Such a "magnetic light" state in a nanohole array should be possible to observe directly using MFM. The estimates show that the total magnetic moment of the nanohole array sample may not exceed $N_{pl}\times\mu_B\sim 10^6\mu_B$ under illumination with 100 mW of the CW 488-nm laser, where N_{pl} is the number of plasmon quanta excited in the array. Such magnetization signals are rather difficult to observe. However, local electromagnetic field enhancement effects often associated with surface plasmon excitation (see discussion later) may facilitate observation of these effects.

In order to detect the relatively weak plasmon-induced magnetism in the nanohole array we have decided initially to sacrifice the high spatial resolution of MFM for the sake of sensitivity. Thus, a custom MFM has been built [Fig. 5(c)] in our laboratory, which uses larger than usual (made of 50-μm radius sharpened Ni wire), and mechanically softer ($\sim 10^{-3}$-N/m force constant) magnetic tips. Images of the local magnetization of a 30×30-μm^{2}array of nanoholes coated with thin polydiacetilene film (similar to the one described in detail in Ref. 4) obtained in zero external magnetic field under illumination with 488-nm circular polarized light are presented in Figs. 5(a) and 5(b). In this experiment the intensity of 488-nm laser light was modulated by a chopper at the frequency, which was chosen to coincide with the lowest mechanical eigenfrequency of the magnetic Ni wire used as a microscope tip. The amplitude of the tip vibration induced by periodically chopped 488-nm illumination has been measured using a conventional optical detection scheme employed for shear-force and atomic force microscopy (AFM)/MFM measurements described in detail in Ref. 18. A lock-in amplifier was used to detect the tip oscillation at the chopper frequency. Based on the $\sim 10^{-3}$-N/m force constant of the tip and the expected plasmon-induced magnetization $\sim 10^6\mu_B$ of the array, the amplitude of tip vibration can be estimated as at least 30 nm, which is easily detectable in the shear-force measurement setup. On the other hand, our test experiments performed in the same experimental geometry with the same sample and with mechanically similar but nonmagnetic wires did not detect any tip vibrations caused by 488-nmnm illumination of the sample. These experiments confirm the magnetic nature of the signal imaged in Figs. 5(a) and 5(b).

Polymer coating causes small shifts in both CSP and the surface plasmon resonances in the wavelength, and increases nonlinear optical properties of the nanohole array due to the large linear and nonlinear dielectric constants of the polymer coating.[4] For example, the lower boundary of the CSP frequencies (the frequency of SP at $k\rightarrow\infty$) is defined by the condition $\epsilon_m(\omega)=-\epsilon_d$, where $\epsilon_m(\omega)$ and ϵ_d are the dielectric constants of the gold and dielectric, respectively [Eq. (1)]. Thus, both resonances are located conveniently with respect to the wavelength range of the set of argon ion laser lines used in the experiment. According to the data on $\epsilon_m(\omega)$ reported in Ref. 19, the shifted CSP peak is located at around 500 nm in this case, so that illumination with 488-nm light must lead to the excitation of CSPs in the nanohole array, while illumination with light at longer wavelengths should not excite CSPs. Characteristic bright and dark stripes indicating magnetic dipole behavior of the entire illuminated nanohole array and some smaller structures within the array are clearly visible in the lower portions of the images in Figs.

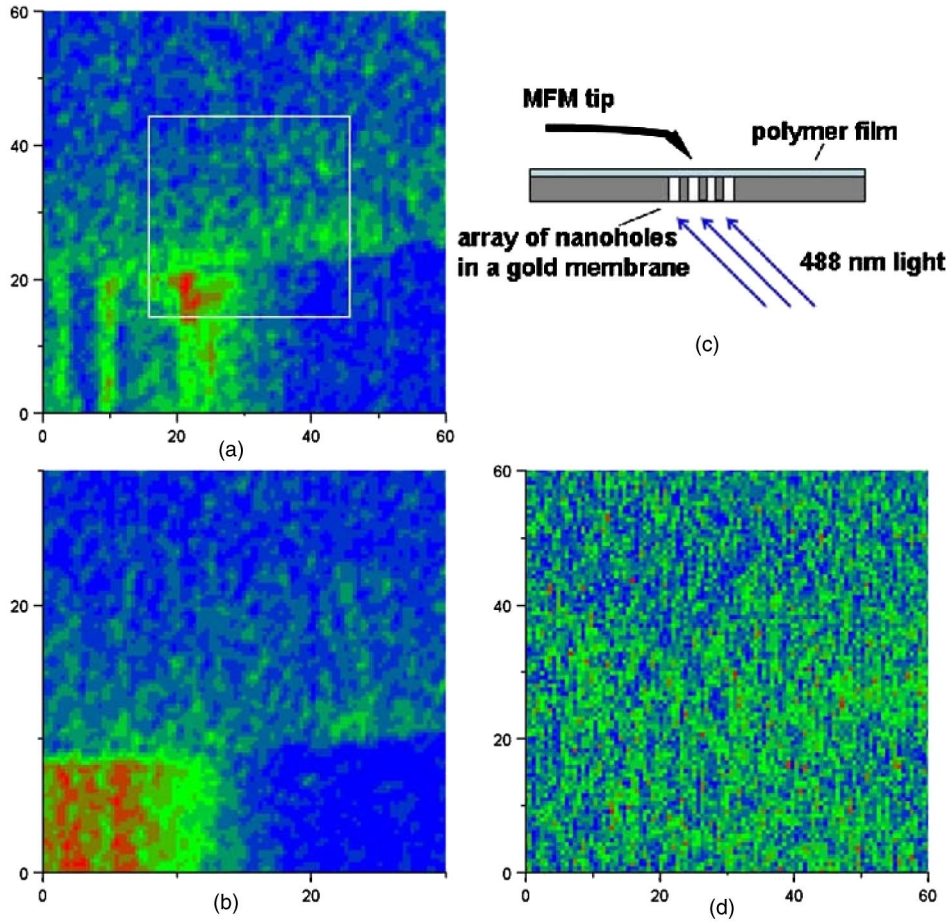

FIG. 5. (Color online) (a) 60×60-μm^2 image of the light-induced magnetization of a 30×30-μm^2 array of nanoholes (located in the bottom left corner of the image) obtained under illumination with 488-nm circular polarized light. The 30×30-μm^2 zoom area shown in (b) is indicated by a square boundary. (c) Schematic of the illumination geometry. (d) Image of the same area obtained with 514-nm light shows no magnetization. In all images red indicates higher value.

5(a) and 5(b) obtained under illumination with 488-nm light. As expected, the observed magnetization signal exhibit rather pronounced spectral behavior. The image in Fig. 5(d) measured outside the presumed CSP resonance under the illumination with 514-nm light over the same area as in Fig. 5(a) shows no magnetization signal. However, the intensity of the 514-nm laser line was four times smaller than the intensity of the 488-nm line. This may have contributed to the observed weakness of illumination-induced magnetism at 514-nm wavelength, even though experiments conducted at 488-nm at four times reduced light intensity detected a small light-induced signal. Thus, evidence of the plasmon-induced magnetization in the nanohole array has been obtained in these experiments.

Fine structure observable in Fig. 5(a) indicates that plasmon-induced magnetization on the scale of a few nanoholes may be detectable in a MFM with higher spatial resolution. In order to check this possibility a commercial Digital Instruments Multimode AFM was modified to allow the transmission of light through the nanohole array. As it appeared from our further work, the magnetic response can be detected even without the additional nonlinearity due to polymer coating. Thus, uncoated nanohole array samples were imaged in lift mode using phase detection with high moment magnetic tips.[20] We have switched to single-period nanohole arrays in these MFM measurements because such arrays are much easier to produce in the gold films using focused ion beam milling. At the same time, such single-period arrays produced reasonable MFM contrast. Figure 6 shows topographical and phase images taken simultaneously on the patterned region of the sample. In Fig. 6(a) the first third of the image was obtained with no sample illumination, the second third then illuminated by a multimode argon-ion laser operating around 488-nm wavelength [all the laser lines were within the broad surface plasmon line shown in Fig. 4(a)], then the last third was obtained with the laser off. Repeating this experiment using a mechanically similar nonmagnetic, metallic tip [Fig. 6(c)] shows no effect, eliminating the possibility that this observation is due to instrumentation artifacts or due to some light-induced force of nonmagnetic origin.

High-resolution images of the local light-induced magnetization are presented in Fig. 7. The ringlike features are clearly visible around the nanoholes in the magnetic image, while no optically induced MFM signal was detected over unmilled regions of the film far from the nanohole array. These ringlike features suggest the picture of surface plasmons as circular currents flowing around the nanoholes. Contrast in the magnetic image was found to be dependent on several factors, including laser power (in accordance with the expectation that the number of SP quanta excited in the structure is proportional to the laser power) and distance between the tip and sample. However, such high-contrast images could be observed only for a few minutes, with the magnetic contrast gradually disappearing. The magnetic contrast in the image could be restored again after the tip remag-

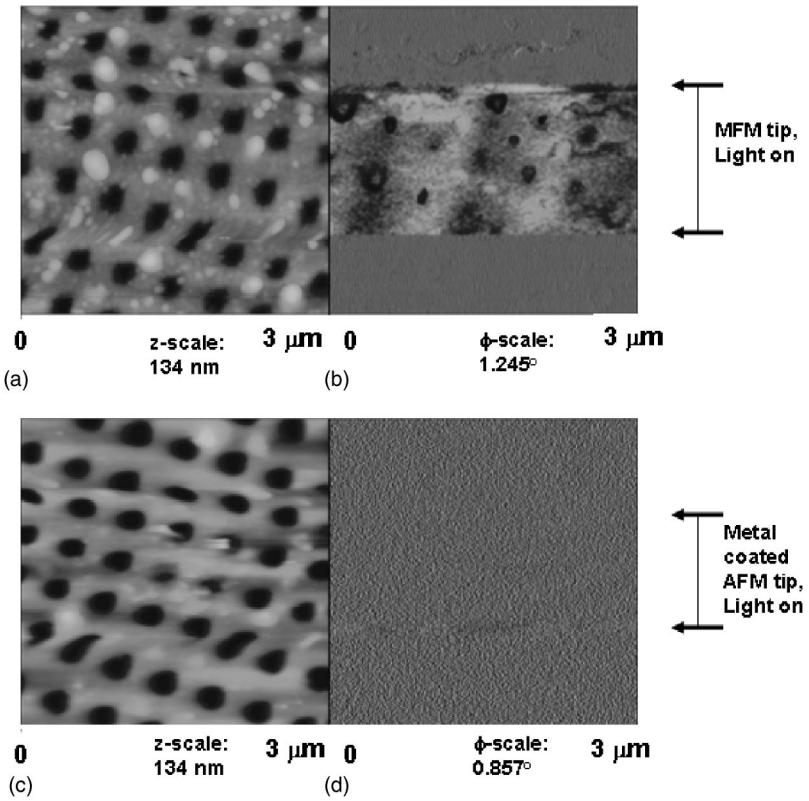

FIG. 6. (a) Nanohole array topography and (b) MFM signal detected in the lift mode using phase detection with high magnetic moment tip. The middle part of the image has been recorded under the illumination with 488-nm laser light; the illumination was switched off in the top and bottom parts of the image. (c) Topography and (d) MFM signal recorded with the mechanically similar metal-coated nonmagnetic tip: there is no difference in the images measured with and without illumination. In all images white indicates higher value.

netization, as shown in Fig. 8. This behavior strongly indicates substantial gradual heating of the magnetic coating of the tip under the intense laser illumination in the experimental setup, which leads to a loss of tip magnetization due to the loss of collinearity of magnetization of individual magnetic domains in the MFM tip. On the other hand, we have checked that the shape of the MFM tips look unchanged in the electron microscope images obtained before and after these measurements. While this effect may be considered as very strong evidence in favor of the magnetic nature of the detected MFM signal, it prevented us from performing more detailed quantitative studies of the plasmon-induced magnetization on such parameters as the illuminating optical power and the tip-sample distance. When the laser power was reduced to the level at which tip-heating effects were no longer considerable, the signal-to-noise level was sufficient only for qualitative observations. On the other hand, the repeatability of our results was tested with ten different MFM tips and six different nanohole array samples. In all these cases the plasmon-induced magnetization has been observed beyond doubt, even though (as often happens in scanning probe microscopy) some tips produced better MFM contrast than the others. For example, the contrast in Fig. 8 is somewhat lower than the contrast observed in Figs. 6 and 7 with a different MFM tip. In addition, the MFM contrast was observed to gradually deteriorate after a prolonged use of the same MFM tip.

While the magnetic nature of the contrast in Figs. 6–8 has been well established, a number of alternative competing mechanisms of nanohole magnetization under external illu-

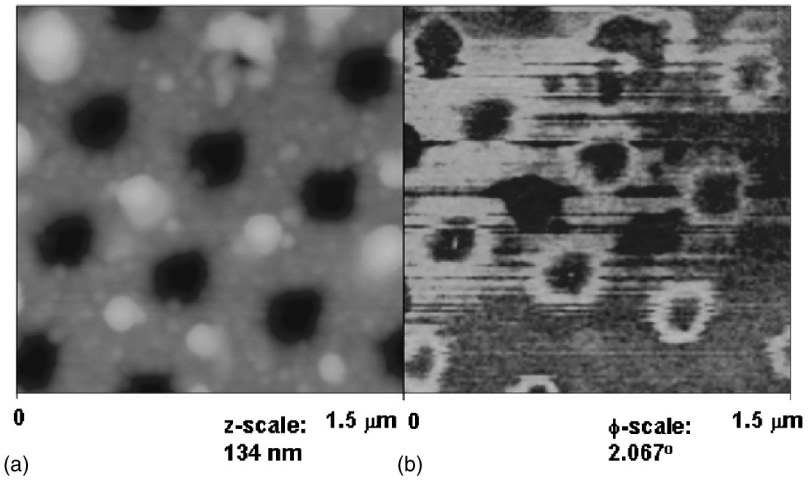

FIG. 7. (a) Topography and (b) high-resolution MFM phase image of the local light-induced magnetization of the nanohole array. In all images white indicates higher value.

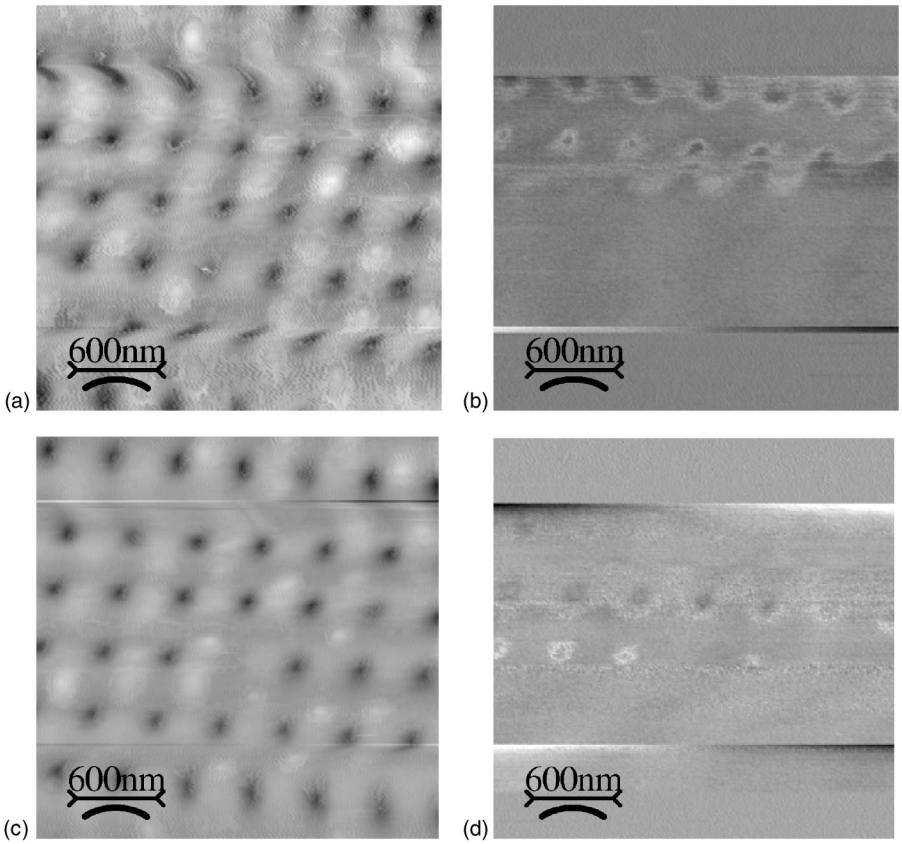

FIG. 8. (a) Nanohole array topography and (b) MFM signal detected using high magnetic moment tip. The middle part of the image has been recorded under the illumination with 488-nm laser light; the illumination was switched off in the top and bottom parts of the images. The magnetic contrast is observed to gradually disappear during the tip illumination. In similar images (c) and (d) measured after the tip remagnetization the magnetic contrast reappears and disappears in a similar manner. This behavior indicates substantial gradual heating of the magnetic coating of the tip under the laser illumination, which leads to a loss of tip magnetization. In all images white indicates higher value.

mination may be considered. One of such mechanisms uses somewhat similar language of surface plasmon excitations in the nanohole array. Illumination of metallic and semiconducting nanostructures with intense light is known to produce simultaneous strong second harmonic generation and photon drag[21] effects, which are the related second-order nonlinear optical effects: sum frequency (2ω) and difference frequency generation processes. The dc electric fields induced by external illumination had been observed previously via measurements of the effect of surface plasmon polariton field on the tunneling current of a scanning tunneling microscope (STM).[22] In these experiments rather large dc voltage ($\sim$1 mV) had been observed over an $\sim$10-nm gap between gold STM tip and sample under the cw 633-nm sample illumination. It was estimated that the fundamental optical field enhancement in the gap of the order of 10^5 was necessary in order to explain this value of the dc electric field. This enhancement is rather typical in metal nanostructures. Similar enhancement factors are observed in other nonlinear optical effects in metal nanostructures, such as the surface enhanced Raman scattering, etc. In our experimental MFM geometry the plasmon-induced dc electric field is effectively screened by the metallic nanostructure, since the sample is illuminated from the back [Fig. 5(c)]. Our estimates of this effect, performed similar to Ref. 22, promise the dc magnetic fields of the order of a few Gauss, based on the 100 mW power of the illuminating fundamental light, expected amplification of the local fundamental optical field of the order of at least 10^2-10^3 in close proximity to the nanoholes, and 10^{-3} typical second harmonic conversion efficiency of metallic nanostructures (second harmonic and dc conversion efficiencies should be of the same order of magnitude). The local dc magnetic fields of such magnitude are easy to detect with a MFM in the phase imaging mode. However, we should emphasize that the language of plasmon magnetic moments and the language of photon drag effect are essentially two different languages to describe the same phenomenon: generation of dc magnetic fields due to plasmon excitation. Another hypothetical possibility to induce magnetic nanoholes is some plasmon-enhanced nonlinear-optical effect in the glass substrate (or polymer coating as in the experiment in Fig. 5). We should point out, however, that the nonlinearities of dielectric near the metal-dielectric interface which supports surface plasmon propagation may be included in the plasmon magnetic moment calculations, and thus, should not be considered as an alternative explanation.

Unfortunately as a rule, the phase changes in the experimental MFM images could not be converted into quantitative data of the magnetic field distribution near the sample of interest. This fact has to do with the complicated shapes of both the sample and the magnetic tip. Magnetic dipole approximation is clearly inaccurate when the tip-sample distance is smaller than characteristic dimensions of the tip and the sample. In general MFM images are interpreted as some linear combination of the sample magnetic field, its gradient, and maybe its higher derivatives.[23] In addition, the effects measured by the MFM tip may result from a combination of direct plasmon-induced magnetization of the sample, and from the plasmon-induced diamagnetic reaction of the sample to the presence of the magnetized MFM tip. According to Eqs. (2) and (13), the relative contribution of these effects is defined by the types of plasmon modes excited in

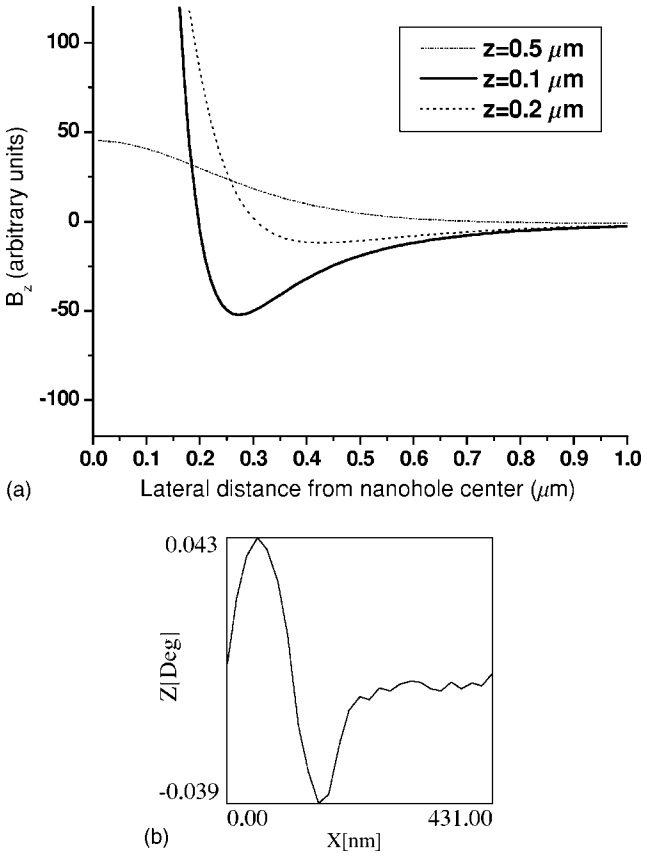

FIG. 9. (a) Results of our calculations of the vertical component of the magnetic field at different distances z from the surface in the model of currents circulating around the nanoholes of the array. The results at $z=100$ nm agree qualitatively with the ringlike structures observed in our experimental MFM images at about the same tip-sample separation, as shown by the cross section of the experimental image shown in (b).

the sample, and by the direction of tip magnetization. The latter factor is known only approximately. From the same equations we may also expect that the diamagnetic response of the sample should be by a factor of $\omega_c/\omega_p \sim 10^{-3}$ weaker than its direct magnetic response, which makes the direct magnetization mechanism more probable. Despite these uncertainties, some qualitative agreement between experimentally measured images and the expected field distribution around nanoholes may be achieved. Figure 9(a) represents results of our calculations of the vertical component of the magnetic field at three different tip-sample separations in the model of currents circulating around the nanoholes of the array. The nanohole size in these calculations is 250 nm, which corresponds to the measured nanohole diameter in the experimental image in Fig. 8(a). The calculation results at $z=100$ nm agree qualitatively with the ringlike structures observed in our experimental MFM images at about the same tip-sample separation, as evidenced by the cross section of the experimental image from Fig. 8(b), which is shown in Fig. 9(b). The contrast in experimental image has been inverted in order to get the best fit. The contrast inversion can be justified by the fact that the sign of the experimental signal depends on the sign of tip magnetization. In addition, the calculation data in Fig. 9(a) show the transition from the ringlike shapes to the simple magnetic field maxima as a function of the effective vertical distance to the rings. Such a behavior may be inferred, for example, from Fig. 8(d).

In summary, we have observed directly the theoretically predicted surface-plasmon-induced magnetization in the array of nanoholes in a metal film. In such metallic nanostructures, propagation of surface plasmons has been observed to depend on the applied external magnetic field. Magnetic force microscopy measurements show that magnetization of the electromagnetic states in a hole array can be achieved by illumination of the structure at the wavelengths corresponding to various surface plasmon excitations. Our finding that zero-point fluctuations of surface plasmon-polariton field may induce considerable magnetism in nanometer-scale metallic samples may be of interest to mesoscopic physics. In addition to the importance of our results to fundamental nanoscience, our observations suggest the possibility to control the transmission of nanoholes at a single-photon level with an external magnetic field. This possibility is extremely attractive in quantum communication applications.

ACKNOWLEDGMENTS

This work has been supported in part by the NSF Grant Nos. ECS-0210438, ECS-0304046, DMR-0348939, 9977530, and by the EPSRC.

[1] H. Raether, *Surface Plasmons* (Springer, Berlin, 1988); A. V. Zayats and I. I. Smolyaninov, J. Opt. A, Pure Appl. Opt. **5**, S16 (2003).
[2] T. W. Ebbesen, H. J. Lezec, H. F. Ghaemi, T. Thio, and P. A. Wolff, Nature (London) **391**, 667 (1998).
[3] S. A. Darmanyan and A. V. Zayats, Phys. Rev. B **67**, 035424 (2003).
[4] I. I. Smolyaninov, A. V. Zayats, A. Stanishevsky, and C. C. Davis, Phys. Rev. B **66**, 205414 (2002).
[5] G. Hackenbroich, Phys. Rep. **343**, 464 (2001).
[6] R. Deblock, R. Bel, B. Reulet, H. Bouchiat, and D. Mailly, Phys. Rev. Lett. **89**, 206803 (2002).
[7] I. I. Smolyaninov, Phys. Rev. B **67**, 165406 (2003).
[8] C. Genet, A. Lambrecht, and S. Reynaud, Phys. Rev. A **67**, 043811 (2003).
[9] K. W. Chiu, and J. J. Quinn, Phys. Rev. B **5**, 4707 (1972).
[10] A. I. Vedernikov, A. O. Govorov, and A. V. Chaplik, JETP **93**, 853 (2001); A. V. Chaplik, JETP Lett. **75**, 292 (2002).
[11] L. D. Landau and E. M. Lifshits, *Electrodynamics of Continuous Media* (Pergamon, New York, 1985).
[12] A. G. Malshukov, Phys. Rep. **194**, 343 (1990).
[13] S. V. Vonsovskii, *Magnetism* (Nauka, Moscow, 1971).
[14] W. Pauli, Z. Phys. **41**, 81 (1927).
[15] L. D. Landau, Z. Phys. **64**, 629 (1930).

[16] G. A. Farias, E. F. Nobre, R. Moretzsohn, N. S. Almeida, and M. G. Cottam, J. Opt. Soc. Am. A **19**, 2449 (2002).
[17] I. I. Smolyaninov, Phys. Rev. D **65**, 047503 (2002).
[18] I. I. Smolyaninov, D. L. Mazzoni, and C. C. Davis, Appl. Phys. Lett. **67**, 3859 (1995).
[19] *Handbook of Chemistry and Physics*, edited by R. C. Weast, M. J. Astle, and W. H. Beyer (CRC, Boca Raton, 1988).
[20] Model MESP-HM high moment magnetic force tips purchased from Digital Instruments.
[21] S. Graf, H. Sigg, K. Kohler, and W. Bachtold, Phys. Rev. B **62**, 10 301 (2000).
[22] I. I. Smolyaninov, A. V. Zayats, and O. Keller, Phys. Lett. A **200**, 438 (1995).
[23] R. Wiesendanger, *Scanning Probe Microscopy and Spectroscopy* (Cambridge University Press, Cambridge, U.K., 1994).